Phase Displaced SVPWM Technique for Five-Phase Open-End Winding Induction Motor Drive

Ramsha Karampuri, Sachin Jain, *Member IEEE*, V. T. Somasekhar, *Member IEEE*
Department of Electrical Engineering,
National Institute of Technology,
Warangal – 506004, INDIA
ramsha_k@nitw.ac.in, jsachin@nitw.ac.in, vtsomasekhar@rediffmail.com

***Abstract*—The three-level dual-inverter connected to Five-Phase Open-End Winding Induction Motor (FPOEWIM) drive can have either isolated DC bus or a single DC bus. The single DC bus configuration is advantageous over the former, since, it avoids the use of bulky isolation transformers. But this configuration adds the zero-sequence current flowing through the common DC bus and the motor phase windings. This paper proposes a SVPWM technique to eliminate the zero-sequence current and also the lower order harmonic currents flowing through the motor phases. The proposed technique operates the dual-inverter using the reference voltage vectors of both the inverters which are phase displaced by 180º. This technique uses the nearest possible space vector locations to realize the resultant reference voltage vector. This could reduce the ripple content in the motor phase current, which in turn reduces the torque ripple. The proposed SVPWM technique not only uses the space vector locations with zero common-mode voltage but also the other locations where the common-mode voltage is not equal to zero. This may lead to the presence of common-mode voltage (approximately 8% of the fundamental), but eliminate the zero-sequence current. The proposed PWM technique along with the system modeling is explained in brief and the simulation results are presented.**

***Keywords—Five-phase Induction Motor; Open-End Winding Topology; Pulse Width Modulation Technique; Space Vector Modulation; Zero-Sequence Current*.**

I. INTRODUCTION

A gigantic research work is being carried out throughout the world to improve the performance and efficiency of an electric drive system for high power electric vehicles. Many researchers have suggested the use of multi-phase machines for these high power applications [1-3]. Multi-phase drives have the advantages of being fault-tolerance, minimized torque ripple, reduced per phase current without increasing the per phase voltage, etc. They also reduce the VA rating of power electronic switches used in the converters because of the reduced per phase current. Further, the overall performance of the drive system may also be improved with the usage of multi-level inverter [4].

Few authors have investigated the multi-phase multi-level drives, especially a three-level dual-inverter connected to Five-Phase Open-End Winding Induction Motor (FPOEWIM) [5-7]. The three-level dual-inverter with Open-End Winding (OEW) configuration has attracted many researches, owing to the advantages such as the absence of neutral point fluctuation, redundancy in the switching states, etc. [8]. The OEW configuration also facilitates to use a single source by using common DC bus or two-isolated sources with separate DC bus. This paper uses a single source connected to dual-inverter through a common DC bus, which could avoid the use of bulky isolation transformers. The use of common DC bus could result in the flow of zero-sequence current which is undesired in a drive system. Recently, Bodo *et. al.* [9, 10] had suggested a Pulse Width Modulation (PWM) technique which eliminates the zero-sequence current in FPOEWIM drive system fed by common DC supply. The authors have suggested to use the space vector locations where exactly the common-mode voltage is equal to zero and proposed two different switching sequences. This technique is similar to the 144º phase displaced SVPWM technique. Most recently, Rajeevan *et. al.* [11] published the work using the same space vector locations as above, but with a different PWM technique to eliminate common mode voltage in both the phase and the pole of dual-inverter.

This paper proposes a 180º phase displaced SVPWM technique, where the reference voltage vectors of inverter-I and inverter-II are phase displaced by 180º. This SVPWM technique uses the space vector locations with the zero common-mode voltage as well as the non-zero common-mode voltage. This may help in minimizing the ripple content in the motor phase current and hence the torque ripple reduces, since the nearest possible space vector locations are used. Further, the proposed technique uses the redundancy in the switching states to reduce the switching frequency thereby reducing the switching losses.

In the following sections, a brief explanation of the system modeling is presented followed by the explanation of proposed SVPWM technique. Thereafter, the simulation results are furnished in the fourth section and then concluded in the last section.

II. SYSTEM MODELLING

The circuit schematic of considered topology with the single DC source connected to three-level dual-inverter fed FPOEWIM drive is shown in Fig. 1. The DC bus voltage of $V_{dc}/2$ is supplied to both the inverters I and II of dual-inverter. The dual-inverter consists of 20 switches in 10 legs (namely *a, b, c, d, e, a', b', c', d' and e'*) which are connected to the either

978-1-4673-7918-2/16 /$31.00 ©2016 IEEE

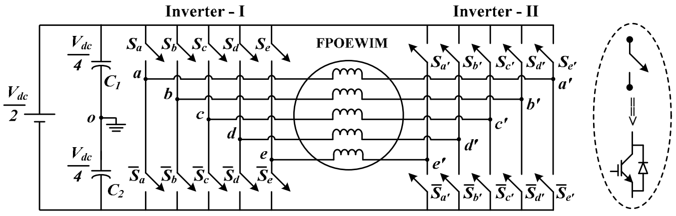

Fig. 1. Three-level dual-inverter connected five-phase open-end winding induction motor drive with single DC source.

ends of FPOEWIM forming the phases *aa′*, *bb′*, *cc′*, *dd′*, *ee′*. The mathematical model of a symmetrical distributed wound FPOEWIM is considered in this paper. The windings are equally displaced by an angle $\theta = 2\pi/5$ with the neutral point opened. The motor model is constructed by considering all the standard assumptions of the general theory of electrical machines. The machine model is represented by a set of stator and rotor phase voltage equilibrium equations referred to a fixed reference frame linked to the stator as:

$$\vec{v}_{kj} = r_j \vec{i}_{kj} + p\vec{\lambda}_{kj} \qquad (1)$$

where, $j = s$ for stator and r for rotor; k = {*aa′*, *bb′*, *cc′*, *dd′*, *ee′*}; $\vec{x}_{kj} = [x_{aa'j} \quad x_{bb'j} \quad x_{cc'j} \quad x_{dd'j} \quad x_{ee'j}]^T$; x = {v (voltage), i (current), λ (flux linkage)}; $\vec{r}_j = diag[r_j \quad r_j \quad r_j \quad r_j \quad r_j]$; and p is the time derivative.

The algebraic flux-linkage equation (2) is obtained from current flowing through the motor phases, the self and mutual inductances of machine winding represented as *L*.

$$\bar{\lambda}_{kj} = \bar{L}\bar{i}_{kj} \qquad (2)$$

The machine model given in (1) and (2) is decoupled into two orthogonal subspaces (*α-β* and *x-y* subspaces) using the Clarke transformation detailed in (3).

$$\bar{C} = \sqrt{\frac{2}{5}}\begin{bmatrix} 1 & \cos\theta & \cos 2\theta & \cos 3\theta & \cos 4\theta \\ 0 & \sin\theta & \sin 2\theta & \sin 3\theta & \sin 4\theta \\ 1 & \cos 2\theta & \cos 4\theta & \cos 6\theta & \cos 8\theta \\ 0 & \sin 2\theta & \sin 4\theta & \sin 6\theta & \sin 8\theta \\ 1/\sqrt{2} & 1/\sqrt{2} & 1/\sqrt{2} & 1/\sqrt{2} & 1/\sqrt{2} \end{bmatrix}\begin{matrix} \alpha \\ \beta \\ x \\ y \\ 0 \end{matrix} \qquad (3)$$

The *α-β* subspace represents the fundamental components responsible for the generation of torque, while the *x-y* subspace includes the third harmonic components which do not contribute to the torque production in a distributed wound FPOEWIM. Fig. 2 shows the space vector locations and switching states in *α-β* and *x-y* subspaces of inverter-I (similar locations and states exists for inverter-II). There exist three groups of vectors large, medium and small with the magnitudes $V_{dc}(\sqrt{5}+1)/10$, $V_{dc}/5$ and $V_{dc}(\sqrt{5}-1)/10$ respectively.

The switching states of inverter-I and inverter-II can be characterized by the vector $[S_a\ S_b\ S_c\ S_d\ S_e]^T$ and $[S_{a'}\ S_{b'}\ S_{c'}\ S_{d'}\ S_{e'}]^T$ respectively, where $S_l \in \{0,1\}$ (l = {*a*, *b*, *c*, *d*, *e*, *a′*, *b′*, *c′*, *d′*, *e′*}). $S_l = 0$ indicates that leg *l* is connected to the negative rail of the DC bus while $S_l = 1$ indicates that leg *l* is connected to the positive rail of the DC bus. The stator phase voltage v_{ks} is obtained from the switching states and the DC bus voltage $V_{dc}/2$ as follows:

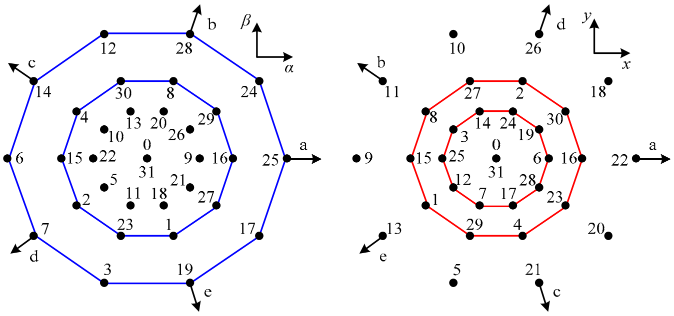

Fig. 2. Space vector locations and switching states for inverter-I in *α-β* and *x-y* subspaces.

$$\begin{bmatrix} v_{aa's} \\ v_{bb's} \\ v_{cc's} \\ v_{dd's} \\ v_{ee's} \end{bmatrix} = \frac{V_{dc}}{10}\begin{bmatrix} 4 & -1 & -1 & -1 & -1 \\ -1 & 4 & -1 & -1 & -1 \\ -1 & -1 & 4 & -1 & -1 \\ -1 & -1 & -1 & 4 & -1 \\ -1 & -1 & -1 & -1 & 4 \end{bmatrix}\begin{bmatrix} (S_a - S_{a'}) \\ (S_b - S_{b'}) \\ (S_c - S_{c'}) \\ (S_d - S_{d'}) \\ (S_e - S_{e'}) \end{bmatrix} \qquad (4)$$

III. Proposed PWM Technique

In case of a five-phase two-level inverter, the *α-β* and *x-y* subspaces consists of 31 space vector locations and 2^5 (=32) switching states as shown in Fig. 2. For a five-phase three-level dual-inverter there exist 211 space vector locations with $2^5 \text{x} 2^5$ (=1024) switching states. For ease of implementing the proposed SVPWM technique, only the medium and large vectors are considered. This helps in reducing the third harmonic component that exist in *x-y* subspace, since, the small vectors in *α-β* subspace are mapped as large vectors in *x-y* subspace and vice-versa, whereas the medium vectors remains the same. Further, choosing only the large and medium vectors also helps in minimizing the number of switching states and the space vector locations. Figs. 3 and 4 show the space vector diagram in *α-β* and *x-y* subspaces for a three-level dual-inverter with large and medium vectors. This results in 141 space vector locations and 484 switching states in *α-β* subspace and 131 space vector locations and 484 switching states in *x-y* subspace in 10 sectors with a span of π/5 radians between each sector.

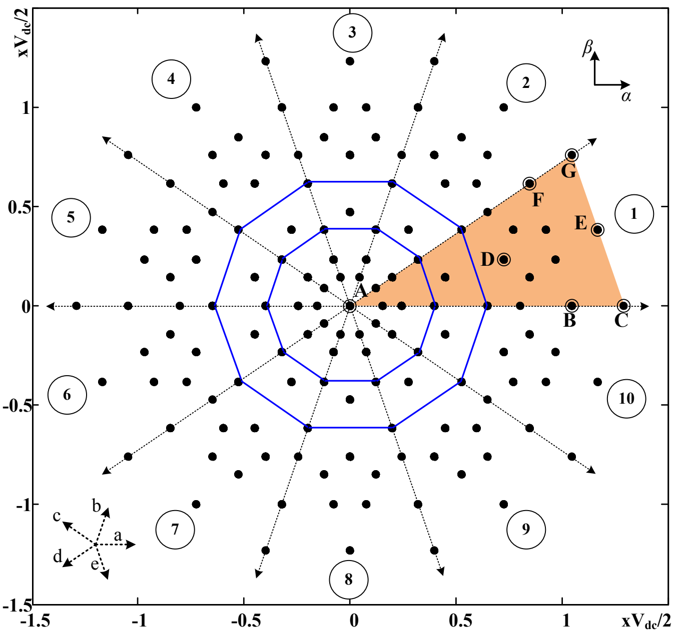

Fig. 3. Space vector locations in *α-β* subspace for the dual-inverter using the medium and large vectors of *α-β* subspace.

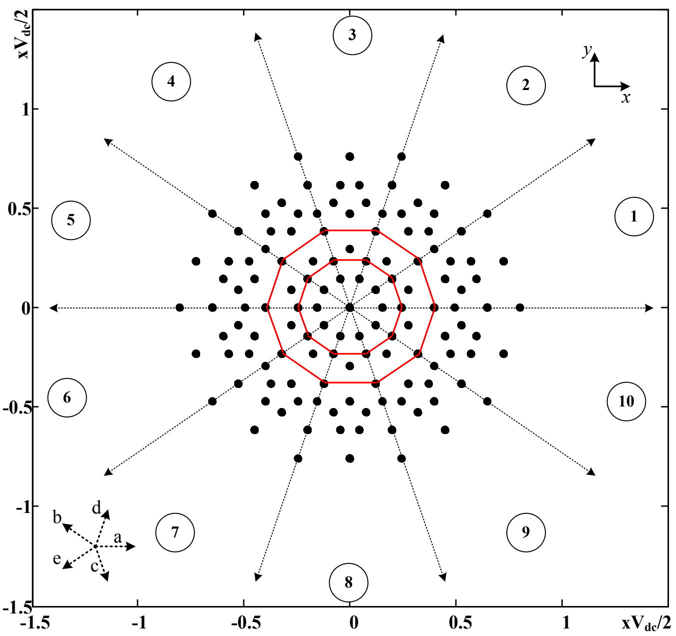

Fig. 4. S pace vector locations in *x-y* subspace for the dual-inverter using the medium and large vectors of *α-β* subspace.

Consider the sector-1 with shaded region as shown in Fig. 3. The proposed SVPWM technique is implemented using the space vector locations A, B, C, D, E, F and G of the shaded sector as encircled in Fig. 3. All the possible switching states at these space vector locations are furnished in Table I. There is a high redundancy in switching states at location A, which can be realized using 22 switching states. Also, there is a redundancy in the switching states at other locations except C and G. The switching states used in the proposed PWM technique are also furnished in the last column of Table I.

The switching sequence in the selected sector (i.e., sector-1) is not unique but changes from sample to sample as shown in Fig. 5. For analysis of the switching sequence, 40 samples per cycle are considered (i.e., 4 samples per sector). Considering the first sample (sample-1) where the reference voltage vector, $\vec{v}_{sr}$ is in phase with the reference, the switching sequence used is A-D-B-E-C-C-E-B-D-A as shown in Fig. 5(a). Similarly, for sample-2 located at 9º the switching sequence is A-D-B-E-E-B-D-A, for sample-3 located at 18º the switching sequence is A-D-E-E-D-A, and for the sample-4 located at 27º the switching sequence is A-D-F-E-E-F-D-A. All the above switching sequences are shown in the respective Figs. 5(a) to (d). From Fig. 5 it can be observed that the reference voltage vector is realized using the nearest possible switching locations, which could help in the reduction of current ripple. Further, the switching locations and the switching sequence are selected such that the third harmonic components in the *x-y* subspace get nullified. For all the remaining sectors the above four switching sequences can be repeated with similar space vector locations in the respective sectors.

To realize the above switching sequences various switching patterns exists based on the redundancy of the switching states. For example, the implementation of switching sequence for sample-1 can be done in four different ways with selected switching states (Table I). These four ways are named as pattern-I, II, III and IV. All the four patterns are given in Table II. The switching pulses generated for these four patterns are shown in Fig. 6. From Fig. 6(a) it can be observed that there is a single switching transition in each leg of the dual-inverter from ON state to OFF state, which corresponds to pattern-I. Whereas, for switching pattern-II, III and IV there are three switching transitions in few legs of the dual-inverter as shown in Figs. 6(b) to (d). This results in the increased switching frequency, which may also lead to the increase in the switching losses. So, to minimize the switching losses, pattern-I is chosen for realizing the reference space vector at sample-1. For realizing the space vectors at samples-2 to 4 in sector-1, the switching sequence and their pattern along with the switching logic are furnished in Table III. From Table III it can be observed that, the state of the switch from ON to OFF is changing in only one leg of each inverter-I and II from one location to the other. The switching transition in each inverter is shown with shading in Table III.

The switching pattern for four samples discussed above not only uses the space vector locations with zero common-mode voltage but also the non-zero common-mode voltage locations. This could improve the THD of the motor phase current by reducing the ripple content and with a compromise in the small quantity of common-mode voltage (approximately 8% of the fundamental). The reduction in current ripple is because of the selection of nearest space vector locations for realizing the reference vector. Further, the phase current ripple reduction results in minimizing the ripple content in the motor generated torque.

TABLE I. SWITCHING STATES AT SELECTED SPACE VECTOR LOCATIONS FOR PROPOSED PWM TECHNIQUE

Space vector location	Possible switching states	Selected Switching states
A	0-0', 1-1', 2-2', 3-3', 4-4', 6-6', 7-7', 8-8', 12-12', 14-14', 15-15', 16-16', 17-17', 19-19', 23-23', 24-24', 25-25', 27-27', 28-28', 29-29', 30-30', 31-31'	0-0', 31-31'
B	16-6', 25-15', 24-14', 17-7'	16-6', 25-15'
C	25-6'	25-6'
D	16-2', 29-15', 28-14', 17-3'	16-2', 29-15'
E	24-6', 25-7'	24-6', 25-7'
F	24-2', 25-3', 29-7', 28-6'	24-2', 29-7'
G	24-7'	24-7'

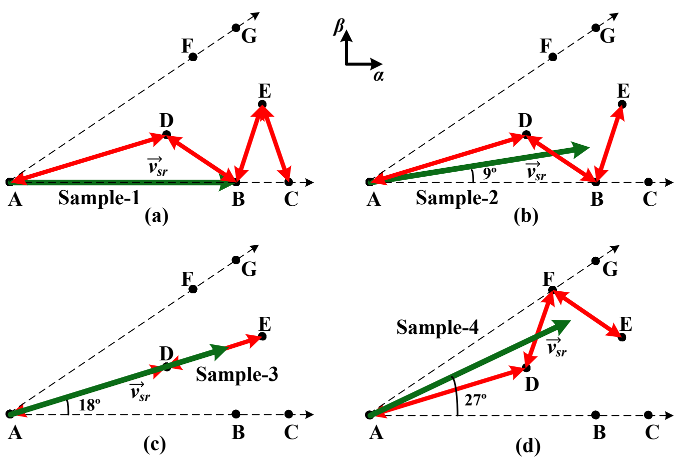

Fig. 5. Switching sequence for realizing the reference voltage vector of the dual-inverter for (a) sample-1, (b) sample-2, (c) sample-3 and (d) sample-4 of sector-1.

TABLE II. FOUR POSSIBLE SWITCHING SEQUENCES FOR REALIZING THE REFERENCE VECTOR AT SAMPLE-1

Pattern	Space vector locations for realizing sample-1								
	A	D	B	E	C	E	B	D	A
I	31-31'	29-15'	25-15'	25-7'	25-6'	24-6'	16-6'	16-2'	0-0'
II	31-31'	16-2'	16-6'	24-6'	25-6'	25-7'	25-15'	29-15'	0-0'
III	31-31'	16-2'	16-6'	24-6'	25-6'	24-6'	16-6'	16-2'	0-0'
IV	31-31'	29-15'	25-15'	25-7'	25-6'	25-7'	25-15'	29-15'	0-0'

TABLE III. SWITCHING SEQUENCE FOR THE PROPOSED PWM TECHNIQUE FOR REALIZING THE REFERENCE SPACE VECTOR IN FIRST SECTOR

Figure	Switching sequence	Switching states used	Switching logic									
			Inverter-I					Inverter-II				
5(a)	A	31-31'	1	1	1	1	1	1	1	1	1	1
	D	29-15'	1	1	1	0	1	0	1	1	1	1
	B	25-15'	1	1	0	0	1	0	1	1	1	1
	E	25-7'	1	1	0	0	1	0	0	1	1	1
	C	25-6'	1	1	0	0	1	0	0	1	1	0
	E	24-6'	1	1	0	0	0	0	0	1	1	0
	B	16-6'	1	0	0	0	0	0	0	1	1	0
	D	16-2'	1	0	0	0	0	0	0	0	1	0
	A	0-0'	0	0	0	0	0	0	0	0	0	0
5(b)	A	0-0'	0	0	0	0	0	0	0	0	0	0
	D	16-2'	1	0	0	0	0	0	0	0	1	0
	B	16-6'	1	0	0	0	0	0	0	1	1	0
	E	24-6'	1	1	0	0	0	0	0	1	1	0
		25-7'	1	1	0	0	1	0	0	1	1	1
	B	25-15'	1	1	0	0	1	0	1	1	1	1
	D	29-15'	1	1	1	0	1	0	1	1	1	1
	A	31-31'	1	1	1	1	1	1	1	1	1	1
5(c)	A	31-31'	1	1	1	1	1	1	1	1	1	1
	D	29-15'	1	1	1	0	1	0	1	1	1	1
	E	25-7'	1	1	0	0	1	0	0	1	1	1
		24-6'	1	1	0	0	0	0	0	1	1	0
	D	16-2'	1	0	0	0	0	0	0	0	1	0
	A	0-0'	0	0	0	0	0	0	0	0	0	0
5(d)	A	0-0'	0	0	0	0	0	0	0	0	0	0
	D	16-2'	1	0	0	0	0	0	0	0	1	0
	F	24-2'	1	1	0	0	0	0	0	0	1	0
	E	24-6'	1	1	0	0	0	0	0	1	1	0
		25-7'	1	1	0	0	1	0	0	1	1	1
	F	29-7'	1	1	1	0	1	0	0	1	1	1
	D	29-15'	1	1	1	0	1	0	1	1	1	1
	A	31-31'	1	1	1	1	1	1	1	1	1	1

The proposed PWM technique as discussed above is quite complex, since the switching sequence and their pattern changes from sample to sample. But, the implementation is simplified by using the unified voltage modulation algorithm proposed in [12] for three-phase two-level inverter. The unified voltage modulation algorithm is a carrier based SVPWM technique. This technique is extended to five-phase two-level inverter and presented in [13]. The unified voltage modulation algorithm for 3-level dual-inverter connected

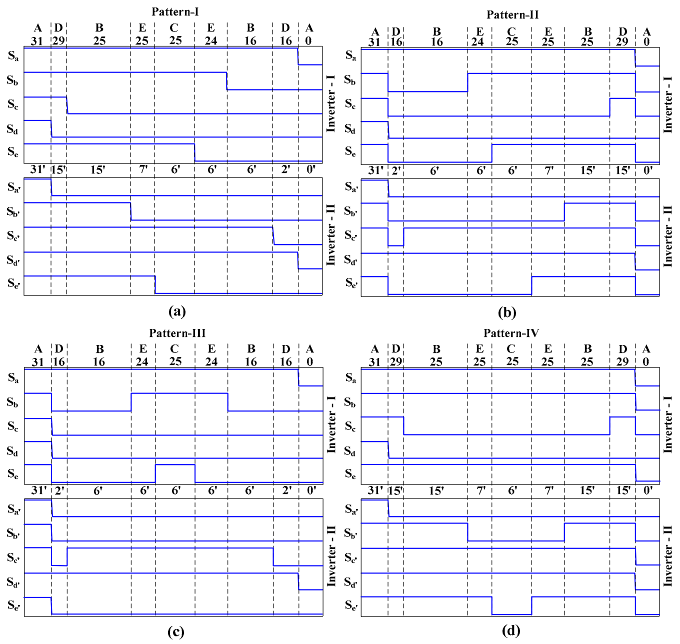

Fig. 6. Switching pulses for inverter-I and inverter-II with (a) pattern-I, (b) pattern-II, (c) pattern-III and (d) pattern-IV.

FPOEWIM is briefly discussed below:

The reference space vector for the dual-inverter is generated using (5)

$$|v_{sr}| = m_a V_{dc} \quad (5)$$

where, m_a is the modulation index.

The proposed PWM technique can be implemented by synthesizing the reference space vector into v_{sr1} for inverter-I and v_{sr2} for inverter-II with 180º phase displacement.

So,

$$|v_{sr}|\angle\delta = \{|v_{sr1}|\angle\delta\} + \{|v_{sr2}|\angle(\pi+\delta)\} \quad (6)$$

where, δ is the angle between the *α-axis* and the reference space vector, which varies in steps by 9º (since 40 samples per cycle are considered).

As the reference voltage vectors are displaced by 180º, the DC bus voltage required is 50% of V_{dc} required in case of conventional five-phase two-level inverter. So, the synthesized space vectors can be written as,

$$\begin{aligned} \vec{v}_{sr1} &= 0.5|v_{sr}|\angle\delta \\ \vec{v}_{sr2} &= 0.5|v_{sr}|\angle(\pi+\delta) \end{aligned} \quad (7)$$

The gating time for top switches of inverter-I (T_{ga}, T_{gb}, T_{gc}, T_{gd} and T_{ge}) are calculated using the unified voltage modulation algorithm presented in [13]. Whereas, the gating time for inverter-II can be calculated as:

$$\begin{aligned} T_{ga'} &= T_s - T_{ga} \\ T_{gb'} &= T_s - T_{gb} \\ T_{gc'} &= T_s - T_{gc} \\ T_{gd'} &= T_s - T_{gd} \\ T_{ge'} &= T_s - T_{ge} \end{aligned} \quad (8)$$

being T_s (= $1/f_s$) the switching time.

The above calculated gating time for inverter-I and inverter-II are then compared with the carrier wave of variable switching frequency, f_s and the PWM pulses are generated. The switching frequency, f_s is calculated as follows:

$$f_s = \frac{N \times m_a \times f_{rated}}{m_{alinear}} \tag{9}$$

where, N is the number of samples considered to be 40; f_{rated} is the rated frequency of the motor i.e., 50Hz; $m_{alinear}$ is the value of the modulation index at the boundary of linear modulation i.e., 1.05.

IV. Simulation Results and Discussion

The simulation of the FPOEWIM drive system using proposed phase displaced SVPWM technique is performed using MATLAB/Simulink. The motor parameters used in the simulation are shown in Table IV. The simulation is performed by considering DC bus voltage of 300V and 40 samples per cycle. The drive is operated with *V/f* control technique along with the proposed SVPWM algorithm.

Figs. 7 to 10 show the simulation results of the system shown in Fig. 1, which is operated with the proposed 180º phase displaced PWM technique. Figs. 7 and 8 show the results at modulation index, m_a set to 0.8. The gating time, T_{ga} calculated using unified voltage modulation algorithm is shown in Fig. 7(a) along with the carrier waveform. By comparing these waveforms the gating signals are generated and given to the dual-inverter. The nature of the gate pulses obtained is same as the pole voltage of the dual-inverter as shown in Fig. 7(b). The performance of the FPOEWIM drive system can be observed from Fig. 8, where the torque and speed plots are shown. The plots in Fig. 8 are captured when the FPOEWIM is started at no-load and the motor is loaded with the load torque of 10N-m at 1.5s.

Figs. 9(a) and (b) shows the FPOEWIM phase current along with its harmonic spectrum when the system is operated with m_a=0.3 and 0.8 respectively. The sinusoidal nature of the phase current depicts the absence of zero-sequence current in the motor phases, which can also be observed from the harmonic spectrum shown below the phase current plots. Also, the third harmonic content in the motor phase current is zero, which is achieved by proper selection of the switching sequence and the pattern as explained in the previous section. Further, the motor phase voltage and its harmonic spectrum are also presented in Figs. 10(a) and (b) for the same modulation indices as above. Form the zoomed part shown in Figs. 10(a) and (b), it can be noted that the 5th harmonic content in the phase voltage is nearly 8% of the fundamental.

The proposed 180º phase displaced SVPWM technique minimizes the ripple content in the motor phase current when compared to the 144º phase displaced SVPWM technique [10]. To verify this, a simulation is performed with the 144º phase displaced SVPWM technique for the similar system with all the parameters given in Table IV. The phase current

TABLE IV. Nominal Parameters of FPOEWIM

Parameter	Value	Parameter	Value
Stator resistance (r_s)	22.63 Ω	Rotor leakage inductance (L_{lr})	35.2 (mH)
Rotor resistance (r_r)	13.1 Ω	Mutual inductance (M)	588 (mH)
Stator leakage inductance (L_{ls})	102 (mH)	Number of poles (P)	6
Moment of inertia (J)	0.148 (kg-m^2)	Nominal speed	100 rad/s

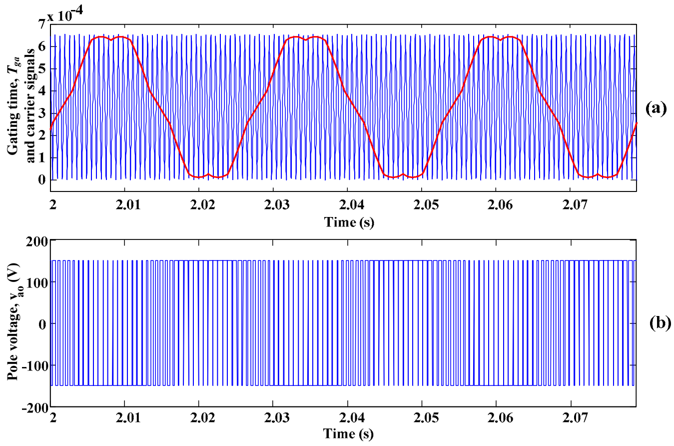

Fig. 7. Simulation results: (a) gating time, T_{ga} and carrier signal; (b) pole voltage, v_{ao} of the inverter-I.

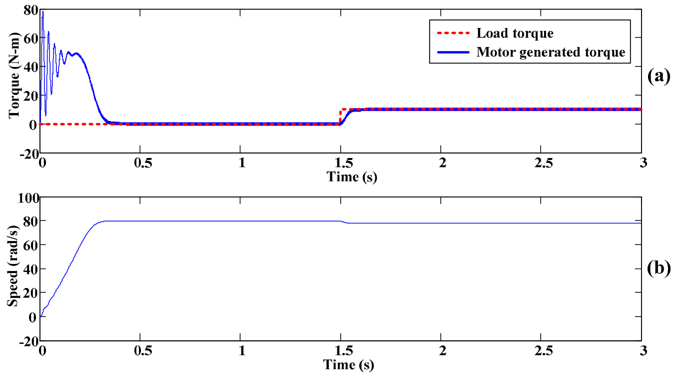

Fig. 8. Simulation results of the FPOEWIM drive system when the load torque of 10N-m is applied at 1.5s: (a) torque and (b) speed.

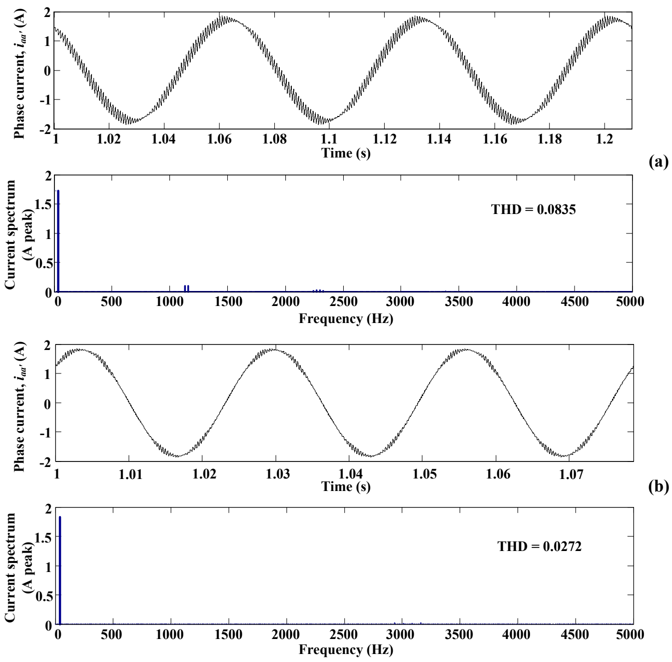

Fig. 9. FPOEWIM phase current, $i_{aa'}$ along with its harmonic specctrum at (a) m_a = 0.3 and (b) m_a = 0.8 (Harmonic spectrum shows that the third harmonic and the zero-sequence current is equal to zero).

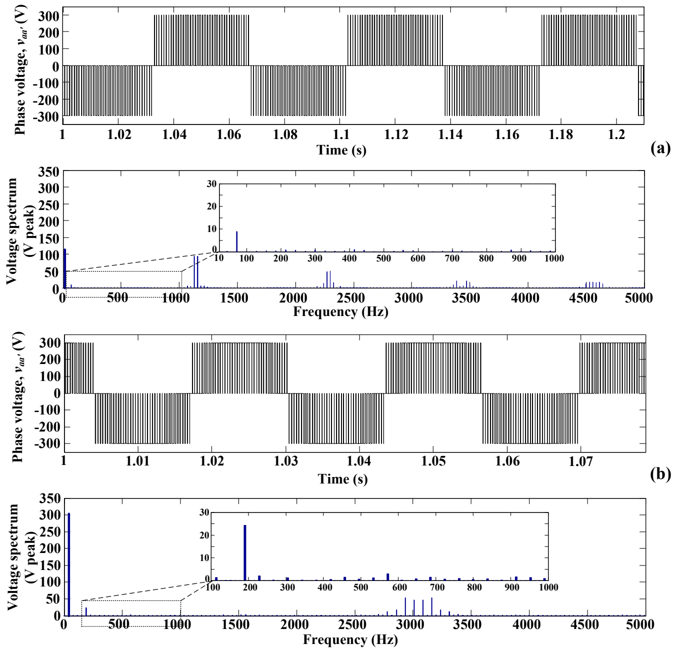

Fig. 10. FPOEWIM phase voltage, $v_{aa'}$ along with its harmonic specctrum at (a) m_a = 0.3 and (b) m_a = 0.8 (Zoomed part: 5th harmonic content is nearly 8% of the fundamental).

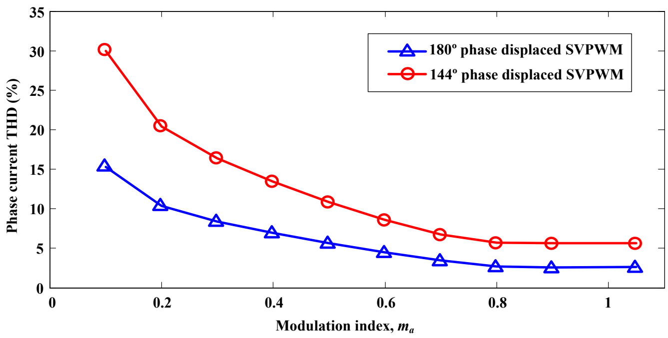

Fig. 11. Comparison of phase current THD for 144º and the proposed 180º phase displaced SVPWM techniques for variation in modulation index from 0.1 to 1.05.

THD values are calculated for various modulation indices varying from 0.1 to 1.05. From Fig. 11, the improvement in the phase current THD using the proposed 180º phase displaced SVPWM technique can be observed.

V. Conclusion

A 180º phase displaced SVPWM technique is proposed for the dual-inverter connected FPOEWIM drive with a single DC source. The detailed analysis and explanation of the proposed technique is presented. A new switching sequence is proposed which varies from sample to sample in a sector. The switching sequence is chosen such that the reference voltage vector at every sample is realized by using the nearest possible space vector locations. This could reduce the ripple content in the motor phase current. In addition, each switching location has the redundancy in the switching states. This redundancy property of the switching states is properly utilized to minimize the switching frequency, thereby reducing the switching losses. The proposed SVPWM technique is implemented using the unified voltage modulation algorithm which is explained in brief. To conclude, the proposed SVPWM technique reduces the ripple content in the motor phase current which in turn helps in the reduction of torque ripple. But one has to compromise with a small quantity of the common-mode voltage (nearly 8% of the fundamental).

References

[1] E. Levi, R. Bojoi, F. Profumo, H.A. Toliyat, S. Williamson, "Multiphase induction motor drives-A technology status review", *IET Elect. Power Appli.*, vol. 1, no. 4, pp. 489-516, 2007.

[2] E. Levi, "Multiphase Electric Machine for Variable Speed Applications", *IEEE Trans. on Industrial Electronics*, vol. 55, no. 5, pp. 1893-1909, 2008.

[3] G. Singh, "Modelling and analysis of six–phase synchronous generator of stand–alone renewable energy generation", *Energy*, vol. 36, no. 9, pp. 5621-5631, 2011.

[4] Akira Nabae, Isao Takahashi, and Hirofumi Akagi, "A new neutral-point-clamped PWM inverter", *IEEE Trans. Ind. Appl.,* vol. IA-17, no. 5, pp. 518-523, Sept./Oct. 1981.

[5] N. Bodo, E. Levi, M. Jones, "Carrier-based modulation techniques for five-phase open-end winding drive topology," *IEEE conf. IECON*, pp. 3656-3651, 2011.

[6] Martin Jones, I. Nyoman Wahyu Satiawan, Nandor Bodo, and Emil Levi, "A Dual Five-Phase Space-Vector Modulation Algorithm Based on the Decomposition Method," *IEEE Trans. on Industry Applications*, vol. 48, no. 6, pp. 2110-2120, Nov./Dec. 2012.

[7] Emil Levi, I. Nyoman Wahyu Satiawan, Nandor Bodo, and Martin Jones, "A Space-Vector Modulation Scheme for Multilevel Open-End Winding Five-Phase Drives," *IEEE Trans. on Energy Conversion*, vol. 27, no. 1, pp. 1-10, Mar. 2012.

[8] H. Stemmler and P. Guggenbach, "Configurations of high-power voltage source inverter drives", *Proc. of EPE conf.*, pp. 7-12, 1993.

[9] N. Bodo, M. Jones, E. Levi, "PWM techniques for an open-end winding five-phase drive with a single DC source supply," *IEEE conf. IECON*, pp. 3641-3646, 2012.

[10] N. Bodo, M. Jones, E. Levi, "A space vector PWM with common-mode voltage elimination for open-end winding five-phase drives with a single DC supply," *IEEE Trans. on Industrial Electronics*, vol. 61, no. 5, pp. 2197-2207, May 2014.

[11] Rajeevan P. P., Haitham Abu-Rub, Atif Iqbal, K. Gopakumar, "Common mode voltage elimination scheme for dual-inverter fed five phase AC drives with open-end stator windings," *IEEE conf. ICIT*, pp. 1680-1685, 2013.

[12] D.-W. Chung, J.-S. Kim and S.-K. Sul, "Unified voltage modulation technique for real-time three-phase power conversion," *IEEE Trans. Ind. Appl.*, vol. 34, no. 2, pp. 374–380, March/April 1998.

[13] Hongwei Gao, Jianyong Su, Guijie Yang, Jian Liu, "SVPWM Equivalent Algorithm Based on Carrier for Five-Phase Voltage Source Inverter," *Conf. Proc. IPEMC*, pp. 758-762, 2012.